Astron. Astrophys. 342, 823–830 (1999)

ASTRONOMY AND ASTROPHYSICS

A near-infrared study of the planetary nebula NGC 2346⋆

B. Vicini[1], **A. Natta**[2], **A. Marconi**[2], **L. Testi**[3], **D. Hollenbach**[4], **and B.T. Draine**[5]

[1] Dipartimento di Astronomia e Scienza dello Spazio, Università degli Studi di Firenze, Largo E.Fermi 5, I-50125 Firenze, Italy
[2] Osservatorio Astrofisico di Arcetri, Largo E.Fermi 5, I-50125 Firenze, Italy
[3] Division of Physics Mathematics and Astronomy, Caltech, MS 105-24, Pasadena, CA 91125, USA
[4] NASA Ames Research Center, MS 245-3, Moffett Field, CA 94035, USA
[5] Princeton University Observatory, Peyton Hall, Princeton, NJ 08544, USA

Received 29 June 1998 / Accepted 5 November 1998

Abstract. This paper presents new near-infrared observations of the planetary nebula NGC 2346. The data include a broad K–band image, an image in the H_2 vibrationally excited 1–0S(1) line and K band slit spectra at three positions in the nebula. In the H_2 1–0S(1) line, the nebula is characterized by a central, bright torus, surrounded by weaker emission with a typical butterfly shape, as seen in Hα and CO lines. The K band spectra show 11 H_2 lines with excitation energies from 6150 to 12552 K. The H_2 data have been compared to the predictions of models which follow the evolution with time of the H_2 emission in PNe of different core mass and shell properties (Natta & Hollenbach 1998). These models compute the emission originating in the photodissociation region (PDR) created at the inner edge of the neutral shell by the UV radiation of the central core, as well as the emission in the shock associated with the expansion of the shell inside the precursor red-giant wind. In NGC 2346, a PDR origin of the H_2 emission in a low-density molecular shell ($n \lesssim 10^4$ cm^{-3}) is indicated. At these low densities, time-dependent H_2 chemistry and X-ray heating of the neutral gas enhance the predicted PDR H_2 line intensity by large factors.

Key words: shock waves – ISM: molecules – ISM: planetary nebulae: individual: NGC 2346 – infrared: ISM: lines and bands

1. Introduction

NGC 2346 is a much studied bipolar planetary nebula at a distance $D \sim 800$ pc (Acker et al. 1992)[1]. At its center lies a binary system, formed by a main-sequence star of spectral type A5V, with mass ~ 1.8 M$_\odot$, temperature ~ 8000 K and luminosity ~ 14 L$_\odot$(Méndez and Niemela 1981; Walsh 1983) and hot star, not detected in the visual, with T$_\star\sim 130000$ K (Méndez 1978), which excites the nebula. Its luminosity is very uncertain, as we will discuss in Sect. 4. Estimates in the literature give L$_\star\sim$ 17–90 L$_\odot$(Méndez 1978; Calvet and Peimbert 1983).

In the optical, the nebula has a butterfly shape (Balick 1987; Walsh et al. 1991), with well developed bipolar lobes and a bright torus which surrounds the central star. The temperature and density of the ionized gas in the torus have been estimated to be $T \sim 12000$ K and $n_e \lesssim 700$ cm^{-3}, respectively (Liu et al. 1995; McKenna & Keenan 1996). The nebula contains a large amount of material in the form of molecular gas, as revealed by the CO observations of Knapp (1986), Huggins & Healy (1986), Healy & Huggins (1988). Bachiller et al. (1989) have mapped the entire nebula in the two CO lines J=1–0 and J=2–1; the morphology of the molecular gas follows very closely that of the ionized gas, showing a clumpy, inhomogeneous torus, tilted with respect to the line of sight by about 56^o, which is expanding outward. Scaled to our adopted distance $D = 800$ pc, the torus has a radius of ∼0.05 pc, and mass ∼ 0.26 M$_\odot$, much larger than the mass of ionized gas (∼0.01 M$_\odot$, Walsh 1983). The radial velocity of the most intense CO condensations is of the order of 15–35 km s^{-1}, which results in a dynamical age of about 2500 yr (but see also Walsh et al. 1991).

NGC 2346 is a Type I nebula, originated by a massive progenitor (Calvet and Peimbert 1983). As many PNe of similar type, NGC 2346 is detected in the vibrationally excited lines of H_2(Webster et al. 1988). Zuckerman & Gatley (1988) have mapped the nebula in the 1–0S(1) line at 2.12 μm using a single-beam 12 arcsec spectrometer with resolution ~ 200. The morphology of the nebula in this line is again very similar to the morphology observed in the optical lines and in CO. This result was confirmed more recently by the images obtained in the same line with much better spatial resolution (about 1–2 arcsec) by Kastner et al. (1994) and Latter et al. (1995).

The excitation mechanism of the vibrationally excited H_2 lines in this, as in other PNe, is still uncertain. Zuckerman & Gatley (1988) discuss the possibility that they form in a shock driven by the fast wind emitted by the central star. Kastner et al. (1994) surveyed a sample of bipolar planetary nebulae (including NGC 2346); they conclude that the H_2 emission very likely originates in thermally excited (possibly shocked) molecular gas. Recently, Natta & Hollenbach (1998; hereafter NH98) have

Send offprint requests to: natta@arcetri.astro.it

⋆ Based on observations obtained at the TIRGO telescope

[1] After this work was completed, a new determination of the distance (D=690 pc) was quoted by Terzian (1997). It is close enough to the value we adopt in this paper that none of the conclusions needed to be changed.

computed theoretical models of the evolution of PN shells and predicted, among others, the intensities of the most commonly observed H_2 vibrationally excited lines (namely, the 1–0S(1) at 2.12 μm and the 2–1S(1) at 2.25μm). They consider the emission of the photodissociation region (PDR) formed by the UV photons emitted by the central star impinging on the shell, including in the calculations time-dependent H_2 chemistry and the effects of the soft X-ray radiation emitted by the central star, which are important in sources like NGC 2346 where $T_\star \gtrsim 10^5$ K. NH98 compute also the emission of the shocked gas at the interface between the shell and the wind ejected by the central star in its previous red giant phase. They point out that both mechanisms (PDR and shocks) can produce lines of similar intensity, with reasonable values of the model parameters.

The PN properties that determine the intensity of the H_2 lines are very different in the two cases. As discussed in NH98, if the emission is produced in the warm, neutral PDR gas, the line intensity depends mostly on the stellar radiation field which reaches the shell and, to a lower degree, on the density of the neutral gas itself. If the emission is produced in the shocked gas, then the line intensity does not depend directly on the properties of the central star or of the PN shell, but only on the shock velocity and on the rate of mass-loss of the precursor red-giant. It is therefore clear that, before attributing any diagnostic capability to the H_2 lines, we need to understand which of the possible excitation mechanisms dominate the PN emission.

This paper is a first attempt to understand the H_2 emission of a well-studied PN in a quantitative way, i.e., by comparing the observations to detailed models of PDR and shock emission, such as those discussed in NH98. To this purpose, we have collected new near-IR broad and narrow-band images of NGC 2346 as well as K band spectra with resolution $\sim$ 1000. These observations are described in Sect. 2. The results are described in Sect. 3 and compared to the predictions of PDR and shock models in Sect. 4. A discussion of the results follows in Sect. 5; Sect. 6 summarizes the main conclusions of the paper.

2. Observations

2.1. ARNICA observations

NGC 2346 was observed during two observing runs in January 1996 using ARNICA (ARcetri Near Infrared CAmera) mounted on the 1.5m TIRGO[2] telescope. ARNICA is equipped with a 256x256 NICMOS3 array, the pixel size with the optics used at TIRGO is $0.96''$; for a complete description of instrument performances, see Lisi et al. (1996) and Hunt et al. (1996). Images were obtained in the K broad-band filter (centered at 2.2 μm) and in a narrow-band filter centered on the 2.12 H_2 1–0S(1) line ($\Delta\lambda/\lambda \sim 1\%$, Vanzi et al. 1998). The seeing was approximately 2–3$''$and the observed field was $\sim 2' \times 2'$, covering all the nebula.

Data reduction was carried out using the IRAF[3] and ARNICA (Hunt et al. 1994) software packages. Photometric calibration in the K band was performed by observing the photometric standards of the FS14 group from the list of Hunt et al. (1997). The quality of the night was rather poor, and the calibration accuracy is estimated to be $\sim 15\%$.

The image in the H_2 1–0S(1) line has been calibrated using the 5 brightest (unsaturated) stars in the ARNICA images, under the assumption that for each star the flux density measured in the line filter was equal to the flux density measured in the K band. Integrated line fluxes on the nebula were then obtained multiplying the flux density by the bandwith of the narrowband filter (Vanzi et al. 1998). The accuracy is $\sim$15%.

2.2. LONGSP observations

K (2.2 μm) band spectra of NGC 2346 were obtained using the LonGSp (Longslit Gornergrat Spectrometer) spectrometer mounted at the Cassegrain focus on the TIRGO telescope. The spectrometer is equipped with cooled reflective optics and grating in Littrow configuration. The detector is a 256$\times$256 engineering grade NICMOS3 array (for detector performances see Vanzi et al. 1995). The pixel sizes are 11.5 Å (first order) and $1''.73$ in the dispersion and slit directions, respectively. LONGSP operates in the range 0.9–2.5 μm achieving a spectral resolution at first order of $\lambda/\Delta\lambda \simeq$950 in K. For a more comprehensive description of the instrument, refer to Vanzi et al. (1997).

Observations were conducted in March 1998 under non-photometric conditions. The slit had dimensions $3''.5\times70''$ and was oriented N-S. The seeing during the observations was in the range 2$''$–4$''$. NGC 2346 was observed at three slit positions labeled as E, S, W and shown in Fig. 1 superimposed on the image in the H_2 1–0S(1) line. Position E and W are centered on the peaks of the line emission located east and west of the central star, respectively (see Zuckerman and Gatley 1988). Position S is centered on the star. At each grating position we performed 5 ABBA cycles (A=on source, B=on sky) with an on-chip integration time of 60 sec, for a total of 10 min integration on source.

Data reduction was performed with the ESO package MIDAS, within the context IRSPEC, modified to take into account LonGSp instrumental characteristics. The frames were corrected for bad pixels, flat-fielded, sky subtracted and wavelength calibrated using the OH sky lines present in all the frames (Oliva & Origlia 1992). After direct subtraction, sky removal was optimized by minimizing the standard deviation in selected areas where the OH sky lines were poorly subtracted but no object emission was present. The wavelength calibration was performed to better than 1/5 of a pixel ($\simeq$2 Å). The spectra were then corrected for telluric absorption by dividing the spectra by the spectrum of the A star BS 2714 after removing its photo-

[2] The TIRGO telescope is operated by the C.A.I.S.M.I.-C.N.R Firenze, Italy

[3] IRAF is made available to the astronomical community by the National Optical Astronomy Observatories, which are operated by AURA, Inc., under contract with the U.S. National Science Foundation

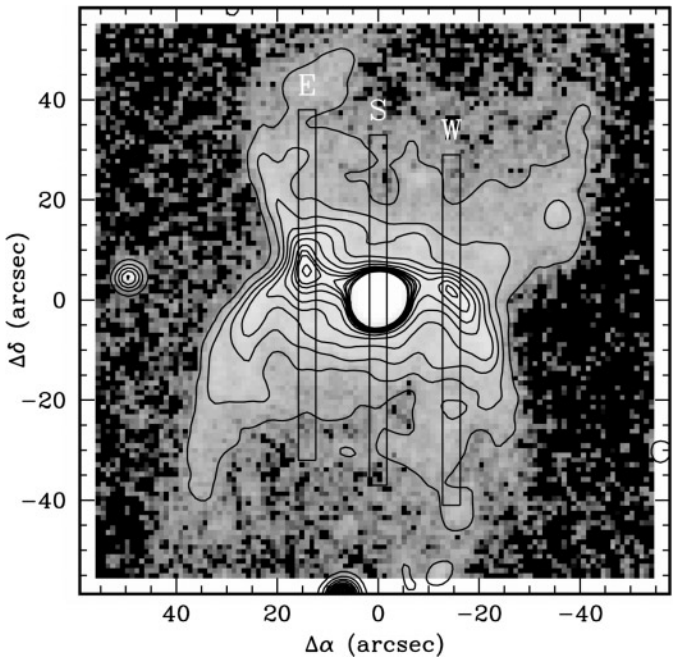

Fig. 1. Image in the H_2 1–0S(1) line. The contours range from 1 to 14 in steps of 1.3×10^{-5} erg cm$-2\,s^{-1}$ sr^{-1}. The three positions of the slit used to obtain the K-band spectra are shown by the black boxes and are marked as E, S and W, respectively. The continuum (not subtracted from the image) is confined to a region of $\sim 5''$ radius centered on the star.

spheric features (mainly Brγ). For more details on LonGSp data reduction, see Vanzi et al. 1997.

Flux calibration of the spectra was achieved by rescaling the observed flux distribution along the slit to match that obtained from the ARNICA image in the 1–0S(1) line at the positions of the slits.

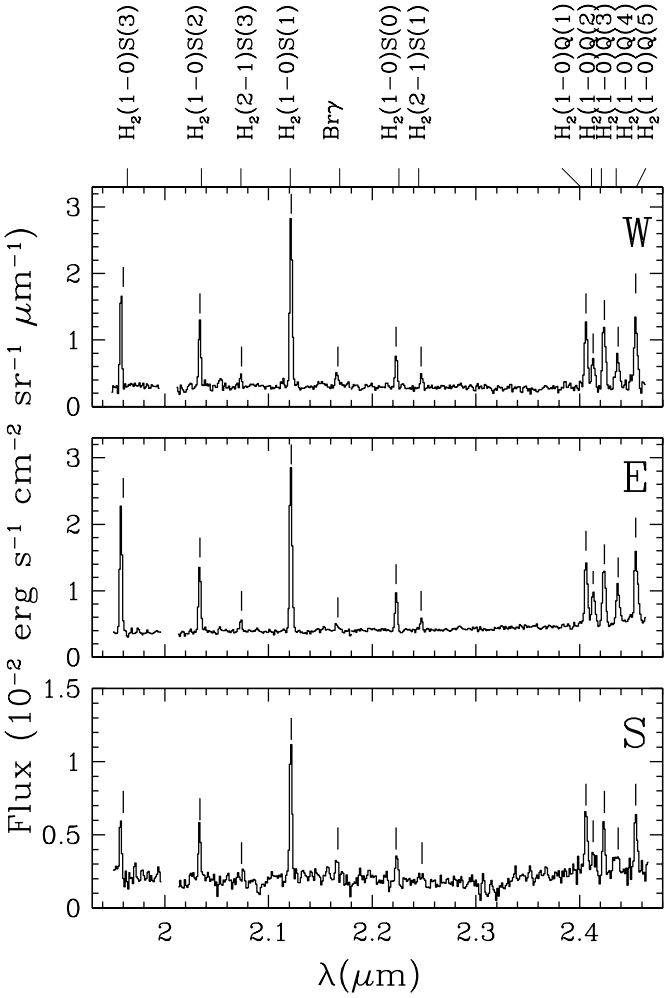

Fig. 2. K-band spectra in the W, E and S positions. The lines have been averaged over a slit section of $\pm 10''$ centered on the peak of the emission (the torus mid-plane). The small gap at $\sim$2–2.04 μm corresponds to a region of very poor atmospheric transmission.

3. Results

The image in the H_2 1–0S(1) line is shown in Fig. 1. As verified with the spectra, the continuum emission is everywhere negligible but at the position of the central star, i.e. in a $5''$ radius region centered on the star.

The H_2 1–0S(1) image of Fig. 1 shows the well-known NGC 2346 morphology, with a bright central region of size $\sim 50'' \times 20''$ and two very extended lobes of weaker emission (Kastner et al. 1994). The central region has two peaks of emission, to the east and west of the star and matches well the bright torus, tilted with respect to the line of sight, seen in optical tracers and in CO (Walsh 1983; Bachiller et al. 1989). The H_2 1–0S(1) intensity is $\sim 1.3 \times 10^{-4}$ erg cm^{-2} s^{-1} sr^{-1}on both peaks. The total luminosity of the nebula in this line is about 0.06 $L_\odot$(for $D = 800$ pc), of which about 48% is contributed by the torus. The average line intensity over the torus (defined as the central region of size $20'' \times 50''$) is $\sim 6 \times 10^{-5}$ erg cm^{-2} s^{-1} sr^{-1}. These numbers are very similar (within 10–20%) to those derived by Zuckerman and Gatley (1988).

The K band spectra in the three positions E, S and W are shown in Fig. 2. The spectra have been averaged over a region of $\sim 20''$ (12 pix) along the slit centered on the torus midplane. The line intensities are given in Table 1, which gives in Column 1 the line identification, in Column 2 the wavelength of the line, in Column 3 the intensity in the W position, in Column 4 that on the E position, in Column 5 that in the S position of the slit. The lines are normalized to the 1–0S(1) line set equal to 100; the intensity of the 1–0S(1) line is given in the table's note. Typical uncertainties on the line ratios are $\sim$10% for ratios $>$50, and $\sim$30% for the others. Lines whose intensity is particularly uncertain are marked with a semicolon.

The variations in intensity along the slit positions E and W and S of the H_2 1–0S(1) and 2–1S(1) lines and of Brγ is shown in Fig. 3. The intensity profiles show that the H_2 emission in the 1–0S(1) line peaks in the torus (i.e., for $|\delta| \lesssim 10''$) and has extended emission with intensity that declines more sharply toward the north than toward the south, possibly due to the tilt in the plane of the sky. Some of the inhomogeneities seen in the

Table 1. K-Band spectrum of the central torus

Line	λ (μm)	W	E	S
1–0S(3)	1.958	50	68	43
1–0S(2)	2.034	36	37	39
He I	2.058	6:	<2	<6
2–1S(3)	2.073	6.2	5.9	9:
1–0S(1)	2.122	100	100	100
2–1S(2)	2.154	<4	<4	<11
Brγ	2.166	8.7	4.7	<16
3–2S(3)	2.201	<4	<4	–
1–0S(0)	2.223	20	21	23
2–1S(1)	2.248	7.0	6.7	<9
3–2S(2)	2.287	<4	<4	–
2–1S(0)	2.355	<4	<4	–
3–2S(1)	2.386	<4	<4	–
1–0Q(1)	2.406	44	44	49
1–0Q(2)	2.415	20	25	<20
1–0Q(3)	2.424	46	41	35
1–0Q(4)	2.437	24	26	<20
1–0Q(5)	2.454	51	55	43

Note: 1–0S(1) intensity 100 corresponds to $7\pm2\times10^{-5}$ erg cm^{-2} s^{-1} sr^{-1} in the W position, $9\pm3\times10^{-5}$ erg cm^{-2}s^{-1} sr^{-1} in the E position and $3\pm1\times10^{-5}$ erg cm^{-2} s^{-1} sr^{-1} in the S position. The spectra have been averaged over a slit portion $\pm10''$ centred on the torus midplane.

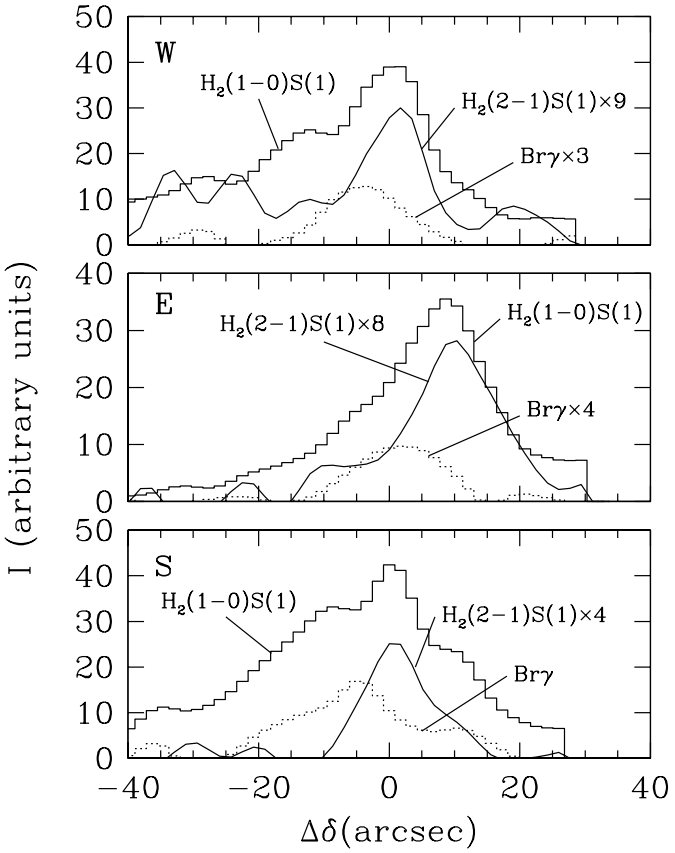

Fig. 3. *Top panel:* variation with declination offset of the intensity of the H_2 1–0S(1) and 2–1S(1) lines and of Brγ (dotted curve) for the slit position E. *Middle panel:* same for slit position W. *Bottom panel:* same for slit position S. All intensity profiles have been smoothed over three pixels. The offset is measured with respect to the central star.

two-dimensional image can also be seen in these profiles. The ratio of the 2–1S(1) over the 1–0S(1) intensity varies between about 0.1 in the W and E peaks of emission to about 0.04 in the condensation detected in the W position $\sim15''$ south of the midplane. Another interesting result which emerges from the spectra and the intensity profiles is that the emission in Brγ extends over the whole central torus. However, Brγ is quite weak, $\sim$10% of the 1–0S(1).

4. Comparison of the H_2 spectrum with models

The H_2 emission in the 1–0S(1) line of the *central torus* of NGC 2346 is compared in this section to the predictions of the NH98 theoretical models.

The NH98 models compute the emission expected from tori (or shells or clumps) exposed to the radiation field of the hot central star and expanding inside the remnant of the wind ejected by the central star in its previous red giant phase. As the central star evolves initially at constant luminosity toward higher effective temperatures and then along the white dwarf cooling track, the torus expands radially with roughly constant velocity and decreasing density. The models consider the effects of UV and soft X-ray radiation on the neutral gas and follow the time dependent chemistry for H_2, solving for the chemical and temperature structure and the emergent spectrum (in the following, the PDR spectrum) of the evolving torus.

The torus expands inside the material ejected by the star in its previous phase as red giant. Since its velocity is larger than that of the wind itself, it gives origin to a shock which heats and compresses the gas, which then emits intense lines of vibrationally excited H_2. NH98 consider the emission of J shocks, since the importance of magnetic field in PNe is not clear and, in this range of shock velocities, the H_2 line intensity is maximum in J shocks.

4.1. PDR models

The NH98 PDR models require the specification of a number of parameters. We fix the mass of the central core, which determines the time scale of the evolution of the stellar radiation field, to be about 0.7$M_\odot$(Calvet and Peimbert 1983; Bachiller et al. 1989). For a core mass $M_\star$=0.7 $M_\odot$, NH98 show the results of only one model, which has a neutral gas density at the time t=2500 yr (roughly the age of NGC 2346) $n_0 \sim 7\times10^5$ cm^{-3}(note that in NH98 the density varies with time as $n = n_0(t/t_0)^{-2}$). We used the NH98 code to compute a number of additional models, varying the $t = 2500$ yr density n_0 from 7×10^3 cm^{-3}(Model 1) to 2.1×10^4 cm^{-3}(Model 2), 7×10^4 cm^{-3}(Model 3) and 7×10^5 cm^{-3}(Model 4). The model parameters are summarized in Table 2. In all cases, He/H=0.13, C/H=5.3×10^{-4}, O/H=4.6×10^{-4}. The results are shown in

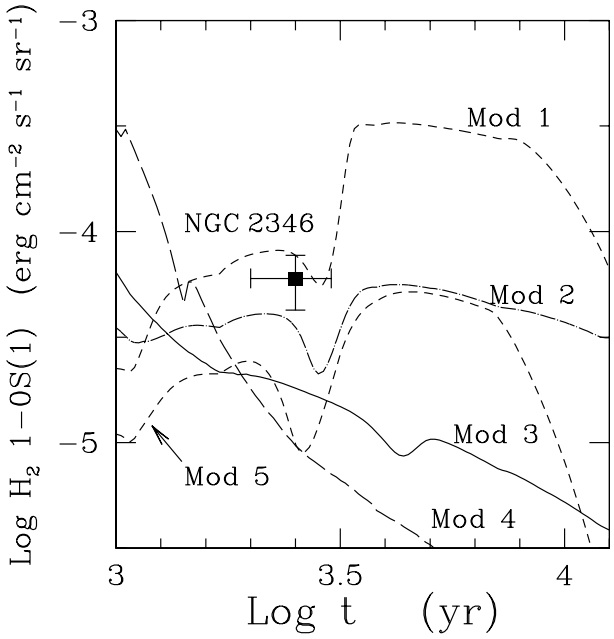

Fig. 4. Model predictions for the H_2 1–0S(1) line intensity as function of the age of the nebula. Model parameters are given in Table 2. All the models have a neutral gas density decreasing as t^{-2} as the torus expands with constant velocity $v = 25\mathrm{km\,s^{-1}}$. The square shows the value of the observed H_2 1–0S(1) intensity averaged over the central torus.

Table 2. Model parameters

	Mod 1	Mod 2	Mod 3	Mod 4	Mod 5
$M_\star/M_\odot$	0.7	0.7	0.7	0.7	[a]
v (km s^{-1})	25	25	25	25	25
n_0 (cm^{-3})	7×10^3	2.1×10^4	7×10^4	7×10^5	7×10^3

[a]: Mod 5 assumes a luminosity of the central core equal to $L_\star(M_\star=0.7)/5$ at all times.

Fig. 4, which plots the intensity of the H_2 1–0S(1) line as a function of time.

The square in Fig. 4 shows the observed intensity of the 1–0S(1) line averaged over the torus. We have estimated the age of NGC 2346 by taking the separation of the two 1–0S(1) peaks (about 30 ″) at $D = 800$ pc and an expansion velocity of ∼25 km s^{-1}(as in the NH98 models), consistent with the observed range (15–35 km s^{-1}) of CO expansion velocity (Bachiller et al. 1989). The result is a dynamical age of ∼2500 yr. The uncertainty on the age is certainly large, but difficult to estimate. We plot in Fig. 4 an error bar corresponding to an uncertainty of ±500 yr. The observed intensity of the 1–0S(1) line is reproduced quite well by the low-density models, especially if we take into consideration the large uncertainties that affect the models as well as the age estimate of the nebula itself.

One problem that arises immediately with these models has to do with the estimated luminosity of the central star. At $t \sim 2500$ yr, a core of 0.7 $M_\odot$ has already reached the white dwarf cooling track; it has a luminosity of about 250 $L_\odot$, an effective temperature $T_\star \sim 1.5\times10^5$ K and a number of ionizing photons $\Phi_i \sim 3\times10^{45}$ photons s^{-1} (Blöcker 1995). While the effective temperature is roughly in agreement with the Zanstra HeII temperature (Méndez 1978), the luminosity is significantly larger than the values 17–90 $L_\odot$ quoted in the literature. However, we are somewhat suspicious of those very low values. The luminosity derived from the HeII λ4685 Å intensity by Méndez (1978) is a lower limit $L_\star$>43 $L_\odot$(for D=800 pc) and is very sensitive to the extinction. The number of ionizing photons we derive from the observed radio flux at 6 cm (86 mJy; Milne and Aller 1975) and from the total Hα flux (Walsh 1983) is at least 2–4 $\times 10^{45}$ photons s^{-1} (assuming no escape of ionizing photons and an average optical depth in H$\alpha \sim 0.7$), consistent with $L_\star$∼250 $L_\odot$, but not with lower values of $L_\star$ (see Fig. 3 of NH98). If $L_\star$=250 $L_\odot$, the non-detection of the white dwarf star in the visual is not surprising; assuming, for simplicity, that the A star and the white dwarf spectrum can be represented by black-bodies at 8500 K and 1.5×10^5 K, having luminosities of 15 and 250 $L_\odot$, respectively, we find that the white dwarf is a factor 54 weaker than the A-type star at 5500 Å, a factor of 10 at 3000 Å and that the two stars become comparable only at ∼2000 Å. This last is consistent with the UV excess (with respect to the flux expected for the A star) measured by the ultraviolet satellite ANS and reported by Méndez (1978). All together, we suspect that the white dwarf luminosity is roughly of the order of 250 $L_\odot$. In any case, we have also computed a model where we have artificially reduced the stellar luminosity by a factor 5 at all times; the density of this model (Model 5), shown as a dashed curve in Fig. 4, is $n_0 = 7\times10^3$ cm^{-3}. The predicted line luminosity scales approximately with the luminosity of the central core. A value $L_\star$=50 $L_\odot$ (although not predicted by any evolutionary track) is still roughly consistent with the observed line intensity, especially if we consider the uncertainty on the PN age estimate.

The best fit to the H_2 1–0S(1) observations is provided by models with low density ($n_0 \sim$ 1–3 $\times 10^4$ cm^{-3}), in good agreement with the low electron density ($\lesssim 10^3$ cm^{-3}) derived for the ionized part of the nebula (Liu et al. 1995; McKenna & Keenan 1996). Assuming pressure equilibrium between the ionized and the neutral gas, and a PDR temperature ∼500 K, we expect a neutral density about 40 times the electron density. The low density we require is in rough agreement with the Bachiller et al. (1989) estimate that the neutral density is $few\times10^3$ cm^{-3}.

In these low-density models, at $t \sim 2500$ yr, the 1–0S(1) emission is mostly due to collisionally excited H_2, kept warm by the heating of the gas by the soft X-rays emitted by the central core. As discussed in NH98, X-rays determine the chemical and physical evolution of the neutral gas around high-mass PN cores, after a short initial phase (about 1000 yr for a 0.7 $M_\odot$ core) where UV photons dominate. If the X-rays effects are neglected, PDR models predict a much lower intensity of the H_2 molecular lines.

Time-dependent effects in the H_2 chemistry are important. For $M_\star$=0.7 $M_\odot$ and $n \propto t^{-2}$, $t \gtrsim 10^3$ yr, the mass of ionized gas increases with time. In these conditions, at each time step a new layer of molecular gas is exposed to the X-ray heating

radiation, as H_2 molecules are advected from deep in the PDR slab toward the irradiated surface. Therefore, compared to the predictions of equilibrium calculations, a larger amount of hot molecular gas is formed, which emits stronger H_2 vibrationally excited lines. This effect, discussed in detail in NH98, is larger in models with lower density, so that the 1–0S(1) intensity is higher in models with lower n. The opposite is true in models where the H_2 chemistry is treated under the assumption of stationary equilibrium. These models predict at $t \sim 2500$ yr a 1–0S(1) line about 7–10 times weaker (for $n_0 \leq 2.1 \times 10^4$ cm^{-3}), mostly due to fluorescence in H_2 pumped by UV photons, and lower in models with lower n.

The predicted intensities of all the H_2 observed lines have been computed using a code which calculates the level population for the N=299 bound states with rotational quantum number $J \leq$29 of the H_2 molecule. The code includes the effects of UV pumping by an external radiation field as well as collisions with H, H_2, He, electrons and protons (Draine & Bertoldi 1996). We have used as input the physical conditions (namely, the radiation field at the inner edge of the PDR and the run with the depth in the PDR of temperature and fractional abundances of H, H_2, He, electrons and protons) computed with the NH98 code for $t = 2500$ yr.

The models agree rather well with the observations for all the lines. Fig. 5 shows a Boltzmann plot for the H_2 transitions, where the column density of the upper level of the transition (divided by its statistical weight) is plotted as function of the energy of the level. The filled dots are the observed values, the open symbols show the prediction of the best-fitting model (Mod 1, $n_0 = 7 \times 10^3$ cm^{-3}). The agreement is somewhat worse for models with higher density, which tend to predict weaker lines from the higher excitation levels.

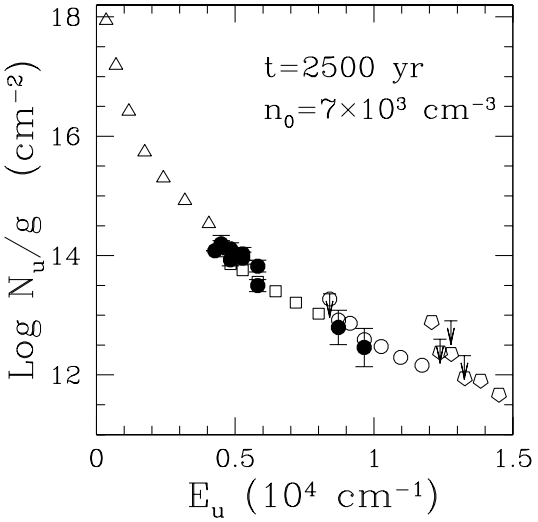

Fig. 5. Boltzmann plot. The values of the column density of the upper level of the transition (divided by its statistical weight) are plotted as function of the energy of the level. The filled dots are the values derived from the observed lines. Arrows are 3σ upper limits. The prediction of the best-fitting model ($n_0 = 7 \times 10^3$ cm^{-3}) are shown by the open triangles for lines of the v=0–0 band, open squares for the 1–0, open circles for the 2–1 and pentagons for the 3–2 band.

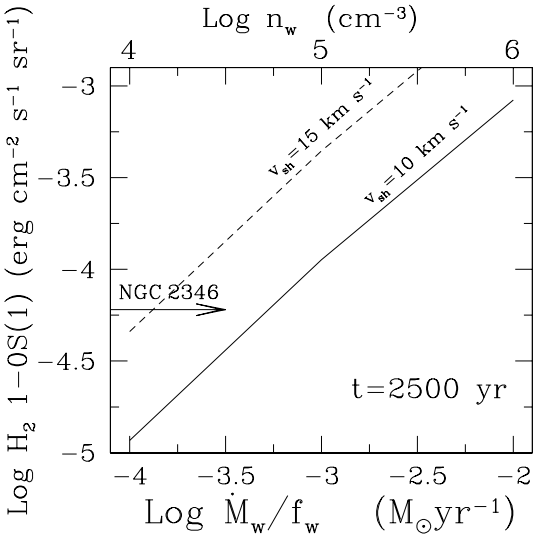

Fig. 6. Intensity of the 1–0S(1) line emitted in the shock between the expanding torus and the precursor red-giant wind at $t = 2500$ yr as function of the red-giant wind parameter $\dot{M}_w/f_w$ (see text). The top scale gives the corresponding value of the pre-shock density n_w for $v_w = 8$ km s^{-1}. The two curves correspond to two values of the shock velocity, as labelled. The observed 1–0 S(1) intensity is shown by the horizontal arrow.

4.2. Shock models

In the NH98 models of the H_2 shock emission, the relevant parameters that determine the intensity of the lines are the shock velocity v_{sh} (i.e., the difference between the torus expansion velocity and the red-giant wind velocity) and the pre-shock density, which, at any given distance R from the star, is determined by the red-giant wind properties ($n_w = \dot{M}_w/(4\pi R^2\, \mu v_w f_w)$, where $\dot{M}_w$ is the rate of mass-loss, v_w the wind velocity, f_w the fraction of solid angle over which the wind was ejected and μ the mean molecular weight). The H_2 line intensity does not depend on the torus properties, but only on its expansion velocity, as long as the matter in the torus does not become completely ionized or photodissociated.

In NGC 2346, the expansion velocity of the neutral gas derived from CO data ranges from ~ 15 to $\gtrsim 35$ km s^{-1}(Bachiller et al. 1989). We show in Fig. 6 the predicted 1–0S(1) intensity at $t = 2500$ yr as a function of the wind parameter $\dot{M}_w/f_w$ and two shock velocities, v_{sh}=10 km s^{-1}(solid line), and v_{sh}=15 km s^{-1}(dashed line). Higher values of v_{sh} will appreciably dissociate H_2 in J shocks. The intensity is computed according to Eq. 17 of NH98. For v_{sh}=10 km s^{-1}, one needs $\dot{M}_w/f_w \sim 4.4 \times 10^{-4}$ M$_\odot$ yr^{-1}in order to reproduce the observed 1–0S(1) intensity. Unless $f_w \ll 0.1$, this implies an unusually high rate of mass-loss in the red-giant wind (Loup et al. 1993). The density of the pre-shock gas (n_w) is about 5×10^4 cm^{-3}; this value is also unconfortably high, given the fact that the observed density of the CO torus (postshock gas), which these models predict to be $\gg n_w$, is $\lesssim 10^4$ cm^{-3} (Bachiller et al. 1989). A lower mass-loss rate is required if the shock ve-

locity is higher. For v_{sh}=15 km s^{-1}, the observed intensity is reproduced by $\dot{M}_w/f_w \sim 1.7\times10^{-4}$ M$_\odot$ yr^{-1}and a pre-shock density of about 2×10^4 cm^{-3}. The shock models of NH98 predict a ratio of the 2–1S(1)/1–0S(1) intensity of 0.10 for $v_{sh} = 10$ km s^{-1}, and 0.19 for $v_{sh} = 15$ km s^{-1}, somewhat larger than the observed value ($\sim$0.07).

5. Discussion

The comparison of the observed intensity of the H_2 1–0S(1) line in the central torus of NGC 2346 to the NH98 model predictions shows that the emission can be produced in the hot PDR generated by the radiation of the central star, once the effect of X-ray heating and time-dependent (advecting) chemistry is taken into account. The best fit is obtained by models with relatively low density of the neutral gas (in agreement with the low density of the ionized material inferred by several authors). However, these PDR models require the luminosity of the hot central star to be significantly higher (L$_\star\sim$250 L$_\odot$) than current estimates.

If the H_2 lines are emitted in the PDR, we expect to observe a similar morphology in the ionized and H_2 emitting gas. In NGC 2346, the PDR origin of the H_2 lines is supported by the fact that the same morphology is seen in H_2 and in Hα (see Walsh 1983). Also, we detect Brγ emission in the two H_2 peaks, with a N-S profile that follows that of the 1–0S(1) line (Fig. 3). The intensity of Brγ predicted by the models is very low, of the order of 8×10^{-6} erg cm^{-2} s^{-1} sr^{-1}, comparable to the observed values (4–6$\times10^{-6}$ erg cm^{-2} s^{-1} sr^{-1}). This supports our estimate of L$_\star$.

In principle, the observed intensity of the H_2 1–0S(1) line can also be accounted for by the emission of the shocked gas produced by the expansion of the torus inside a precursor red-giant wind. However, we estimate (following NH98) that one needs a rather high value of the mass-loss rate in the red-giant wind ($\dot{M}_w/f_w \gtrsim 10^{-4}$ M$_\odot$ yr^{-1}). This, in turn, implies a high density of the pre-shock gas ($\gtrsim 10^4$ cm^{-3}), which is not supported by any existing observation. In fact, as discussed by Zuckerman and Gatley (1988), the main difficulty in ascribing the H_2 vibrationally excited emission to shocks comes from the high momentum rate these models require. Many authors (see the review by Kwok 1993) have proposed that the formation and expansion of the PN shell (or torus) is related to the action of the fast wind from the central star. In this case, the ambient gas (pre-shock red giant wind) gains momentum approximately at the rate at which momentum is delivered to the torus by the fast wind. Since the fast wind is radiation driven, this rate ($\dot{P}$) must be $\lesssim$L$_\star/c$. In NGC 2346, we estimate that $\dot{P}$ is at least $\sim 2\times10^{28}$ erg cm^{-1} s^{-2}, i.e., more than 600 times the present value of L$_\star/c$ (for L$_\star$=250 L$_\odot$) and 12 times higher than the maximum L$_\star$/c reached by the star in its earlier evolution, according to the evolutionary tracks of Blöcker (1995).

The interpretation of the H_2 emission in terms of shocks is often justified in the literature by the low measured ratio of the 2–1S(1) to the 1–0S(1) intensity. This argument, however, is not very strong, since in dense PDRs the low vibrational H_2 levels are thermalized. The PDR models discussed in Sect. 4.1 predict a ratio 2–1S(1)/1–0S(1)$\sim$0.15 (not very different from the 0.10–0.18 range predicted by shock models; see Sect. 4.2), independently of the density and stellar luminosity. These values are somewhat higher than the observed ratio ($\sim$0.07). It is possible, and worth further investigations, that models tend to overestimate the fluorescent component of high vibrational lines, possibly because of uncertainties in the collisional deexcitation rates.

An interesting result of our observations, and one that we cannot account for with our simple models, is the variation of the 2–1S(1)/1–0S(1) ratio with position along the slits, ranging from about 0.08 to 0.15 along the W slit, and from 0.08 to 0.23 along the E slit (see Fig. 3). These variations are not monotonic with the distance from the peaks, but show evidence of structures, especially along the W slit. It is possible that this is due to density variations, which affect the fluorescent contribution to the 2–1S(1) line. If the emission is due to shocks, this could trace variations in the propagation velocity of the shock in an inhomogeneous medium.

Further support to the PDR origin of the H_2 emission can be obtained by observing lines from higher vibrational states. We show in Table 3 PDR model-predicted values for lines not detected so far in NGC 2346, which, however, are accessible from space. The lines are very weak with respect to the 1–0S(1), with ratios that do not depend significantly on the density. We expect that they will be substantially weaker in shocks. To complete the discussion of the H_2 spectrum, we show in Table 4 model-predicted values of the intensity of mid-infrared lines in the v=0–0 band for four of the PDR models described in Sect. 4.1. These lines have been observed by ISO in a number of PNe (among them NGC 2346; Barlow et al. in preparation), and may be useful diagnostic of the physical conditions (see NH98).

Table 3. High-v H_2 PDR predicted line ratios

Line	λ (μm)	Mod 1	Mod 2	Mod 3	Mod5
		(1–0S(1)=100)			
4–3S(1)	2.5414	15	20	20	18
5–4S(1)	2.7172	0.6	0.8	0.8	0.7
6–5S(1)	2.9207	0.2	0.3	0.3	0.3

Table 4. Mid-Infrared H_2 PDR predicted line intensities

Line	λ (μm)	Mod 1	Mod 2	Mod 3	Mod5
		(10^{-5} erg cm^{-2} s^{-1} sr^{-1})			
0–0S(0)	28.22	0.07	0.06	0.03	0.05
0–0S(1)	17.03	1.4	1.3	0.6	1.2
0–0S(2)	12.28	0.8	1.0	0.6	0.7
0–0S(3)	9.66	2.8	3.1	2.5	1.9
0–0S(4)	8.02	1.3	1.0	0.9	0.5
0–0S(5)	6.90	5.0	2.7	1.9	1.0
0–0S(6)	6.11	1.7	0.7	0.4	0.3

6. Summary and conclusions

This paper is motivated by our interest in understanding the origin of the H_2 emission in PNe. Recently, Natta & Hollenbach (1998) have computed the evolution with time of the H_2 emission expected in PNe of different core mass and shell (or torus) properties. Their models compute the emission originating in the photodissociation region (PDR) created by the UV radiation of the central core incident on the inner edge of the neutral shell, as well as the emission in the shock associated to the expansion of the torus inside the precursor red-giant wind. NH98 show that both regions can produce intense H_2 emission and that detailed studies of individual PNe are necessary.

NGC 2346 is a good candidate. It is a bright, young PN, with a typical butterfly morphology characterised by well developed bipolar lobes of emission and a bright torus around the central star. The same morphology is seen in Hα, CO and in the H_2 1–0S(1) line. There is a large amount of information in the literature, concerning the properties of the ionized region and the gas kinematic that can be used in our analysis.

We have collected near infrared observations of NGC 2346. The data include broad K band image, an image in the H_2 vibrationally excited 1–0S(1) line and slit spectra in the K band in three positions in the nebula. The images confirm the well-known NGC 2346 morphology, with a central, bright torus, surrounded by weaker emission with a typical butterfly shape. The K band spectra show 11 H_2 lines with excitation energies from 6150 to 12552 K. Profiles of the lines intensity along the slit show evidence of secondary condensations outside the torus midplane.

A comparison of our observations with the NH98 models shows that PDR emission can account for the H_2 observations. This requires a low-density shell ($n \lesssim 10^4$ cm^{-3}), in agreement with the low density measured in the ionized region. Note that steady-state models or models where the soft X-ray radiation from the star is ignored predict a 1–0S(1) intensity one order of magnitude lower than models where both these effects are included. PDR models of the H_2 emission needs a central star significantly more luminous than estimated in the literature (250 $L_\odot$ against 17–90 $L_\odot$). However, we think that this is consistent with all the available data, including our own Brγ observations.

It is unlikely that the H_2 emission originates in the shock between the expanding shell and the precursor red giant wind. Shock models require a much larger momentum input to the torus than possible from the central star. We estimate the discrepancy to be at least a factor 600 for the current luminosity of the central star (taken to be 250 $L_\odot$) and a factor 12 if we consider the maximum luminosity ever reached by the star in its previous evolution.

In conclusion, we have proved that the PDR origin for the H_2 emission in NGC 2346 is likely and that the models, even if very simple, can account for a number of the observed properties. We suggest some additional observations of lines from higher excitation vibrational levels and in the 0–0 band, which may help in determining the physical conditions in the shell with higher accuracy.

Acknowledgements. We thank Leonardo Vanzi for his help during observations, Sandro Gennari and the LONGSP/TIRGO staff for their help in this project. We are indebted to Frank Bertoldi, Tino Oliva and Malcolm Walmsley for many interesting discussions on the various aspects of this work. The theoretical project on time-dependent PDR was partly supported by ASI grants 92-RS-54, 94-RS-152, ARS-96–66 to the Osservatorio di Arcetri. Support from C.N.R.–N.A.T.O. Advanced Fellowship program and from NASA's *Origins of Solar Systems* program (through grant NAGW–4030) is gratefully acknowledged.

References

Acker A., Ochsenbein F., Stenholm B., et al., 1992, Strasbourg-ESO Catalogue of Galactic Planetary Nebulae. ESO
Bachiller R., Planesas P., Martin-Pintado J., Bujarrabal V., Tafalla M., 1989, A&A 210, 366
Balick B., 1987, AJ 94, 671
Blöcker T., 1995, A&A 299, 755
Calvet N., Peimbert M., 1983, Rev. Mex. Astron. Astrofis. 5, 319
Draine B.T., Bertoldi F., 1996, ApJ 468, 269
Huggins P.J., Healy A.P., 1986, ApJ 346, 201
Healy A.P., Huggins P.J., 1988, AJ 95, 866
Hunt L.K., Lisi F., Testi L., et al., 1996, A&AS 115, 18 1
Hunt L.K., Mannucci F., Testi L., et al., 1998, AJ 115, 2594
Hunt L.K., Testi L., Borelli S., Maiolino R., Moriondo G., 1994, Technical Report 4/94, Arcetri Astrophysical Observatory
Kastner J., Gatley I., Marrill K.M., Probst R., Weintraub D., 1994, ApJ 421, 600
Knapp G.R., 1986, ApJ 311, 371
Kwok S., 1993, ARA&A 31, 63
Latter W.B., Kelly D.M., Hora J.L., Deutsch L.K., 1995, ApJS 100, 159
Lisi F., Hunt L.K., Baffa C., et al., 1996, PASP 108, 364
Liu X.-W., Barlow M.J., Danziger I.J., Clegg R.E.S., 1995, MNRAS 273, 47
Loup C., Forveille T., Omont A., Paul J.F., 1993, A&AS 99, 291
McKenna F.C., Keenan F.P., 1996, PASP 108, 610
Méndez R.H., 1978, MNRAS 185, 647
Méndez R.H., Niemala V.S., 1981, ApJ 250, 240
Milne D.K., Aller L.H., 1975, A&A 38, 183
Natta A., Hollenbach D., 1998, A&A 337, 517
Oliva E., Origlia L., 1992, A&A 254, 466
Terzian Y., 1997, In: Habing H.J.,Lamers H.J.G.L.M. (eds.) IAU Symp.180 on Planetary Nebulae. p. 29
Vanzi L., Gennari S., Ciofini M., Testi L., 1998, Experimental Astronomy, in press.
Vanzi L., Marconi A., Gennari S., 1995, In: Davis Philip A.G., et al. (eds.) New Developments in Array Technology and Applications. p. 231
Vanzi L., Sozzi M., Marcucci G., et al., 1997, A&AS 124, 573
Walsh J.R., 1983, MNRAS 202, 303
Walsh J.R., Meaburn J., Whitehead M.J., 1991, A&A 248, 613
Webster B.L., Payne P.W., Storey J.W.V., Dopita M.A., 1988, MNRAS 235, 533
Zuckerman B., Gatley I., 1988, ApJ 324, 501